

1 **Novel epitopes of human monoclonal antibodies targeting the influenza virus**
2 **N1 neuraminidase**

3
4 **Ericka Kirkpatrick Roubidoux^{1,2}, Meagan McMahon¹, Juan Manuel Carreño¹, Christina**
5 **Capuano¹, Kaijun Jiang¹, Viviana Simon^{1,3,4}, Harm van Bakel^{5,6}, Patrick Wilson⁷, Florian**
6 **Krammer¹**

7
8 ¹*Department of Microbiology, Icahn School of Medicine at Mount Sinai, New York, NY*

9 ²*Graduate School of Biomedical Sciences, Icahn School of Medicine at Mount Sinai, New York, NY*

10 ³*Global Health Emerging Pathogens Institute, Icahn School of Medicine at Mount Sinai, NY, USA*

11 ⁴*Division of Infectious Diseases, Department of Medicine, Icahn School of Medicine at Mount Sinai, New*
12 *York, NY, USA*

13 ⁵*Department of Genetics and Genomic Sciences, Icahn School of Medicine at Mount Sinai, New York, New*
14 *York, USA*

15 ⁶*Icahn Institute for Data Science and Genomic Technology, Icahn School of Medicine at Mount Sinai, New*
16 *York, New York, USA*

17 ⁷*Department of Medicine, Section of Rheumatology, the Knapp Center for Lupus and Immunology,*
18 *University of Chicago, Chicago IL*

19
20
21 **Abstract**

22 Influenza virus neuraminidase (NA) targeting antibodies are an independent correlate of
23 protection against infection. Antibodies against the NA act by blocking enzymatic activity,
24 preventing virus release and transmission. As we advance the development of improved
25 influenza virus vaccines that incorporate standard amounts of NA antigen, it is important to
26 identify the antigenic targets of human monoclonal antibodies (mAbs). Additionally, it is
27 important to understand how escape from mAbs changes viral fitness. Here, we describe
28 escape mutants generated by serial passage of A/Netherlands/602/2009 (H1N1) in the
29 presence of human anti-N1 mAbs. We observed escape mutations on the N1 protein around
30 the enzymatic site (S364N, N369T and R430Q) and also detected escape mutations located on
31 the sides and bottom of the NA (N88D, N270D and Q313K/R). We found that a majority of

32 escape mutant viruses had increased fitness *in vitro* but not *in vivo*. This work increases our
33 understanding of how human antibody responses target the N1 protein.

34

35 **Importance**

36 As improved influenza virus vaccines are being developed, the influenza virus neuraminidase
37 (NA) is becoming an important new target for immune responses. By identifying novel epitopes
38 of anti-NA antibodies, we can improve vaccine design. Additionally, characterizing changes in
39 viruses containing mutations in these epitopes aids in identifying effects of NA antigenic drift.

40

41 **Introduction**

42 Influenza viruses cause seasonal epidemics and, occasionally, global pandemics, that lead to
43 significant morbidity and mortality worldwide (1, 2). They are a member of the family
44 *Orthomyxoviridae* and contain a segmented, negative sense RNA genome. Two of the genetic
45 segments encode for the glycoproteins present on the viral surface, the hemagglutinin (HA) and
46 the neuraminidase (NA) (3, 4). The HA of influenza viruses, which is responsible for receptor
47 binding and viral entry, has been largely credited as the immunodominant target of the
48 immune response after vaccination and natural infection (3-5). The NA acts as a sialidase,
49 removing terminal sialic acids and allowing for viral egress and spread. To function properly, the
50 NA must be present on the viral surface as a homo-tetramer (6-8).

51 Seasonal influenza virus vaccines are the first line of defense against infection (9). Typically,
52 these vaccines are standardized based on the HA content but have varying NA content with
53 unknown structural integrity (10, 11). In addition, seasonal vaccines can have varying

54 effectiveness from 20% to 60% in a given year (12, 13). Low vaccine effectiveness can be largely
55 attributed to antigenic variability of the HA vaccine component compared to circulating strains
56 (14-17). It may be possible to improve seasonal vaccine effectiveness by including a standard
57 amount of a second viral antigen, the NA (18, 19). It has recently become appreciated as an
58 additional important target of anti-influenza virus immunity (18-21). During natural infection,
59 antibodies targeting both the HA and the NA are produced, however NA antibodies are rarely
60 detected after vaccination (10). NA specific antibodies have been demonstrated to prevent
61 severe infections, restrict transmission and protect from lethal challenge in the mouse model
62 (8, 22-27). These antibodies function as neuraminidase inhibitors by blocking the NA enzymatic
63 site and preventing viral spread (10, 22).

64 Residues critical for NA inhibiting antibodies were first characterized using murine antibodies
65 (28-30). The monoclonal antibody (mAb) CD6 was found to span the dimer interface, while
66 other mAbs were found to only bind to a single monomer. Additional work has been ongoing to
67 identify targets of human mAbs (10, 31-33). A majority of these residues can be attributed to
68 the discovery of broadly-reactive NA mAbs that target the enzymatic site (33). Interestingly, few
69 residues have been identified as targets of both human and murine mAbs. This emphasizes the
70 importance of using human anti-N1 mAbs to define true antigenic sites on the N1 protein. The
71 targets of several previously published mAbs have yet to be defined, leaving a gap in our
72 understanding of human mAb epitopes. Here, we use a panel of these uncharacterized mAbs to
73 determine additional N1 residues targeted by human anti-N1 mAbs. The mAbs used in this
74 study were isolated from individuals that were naturally infected and have varying levels of
75 cross-reactivity and NAI activity (10).

76

77 **Results**

78 **Generation of N1 mAb escape mutant viruses**

79 For epitope analysis, we chose a panel of N1 specific mAbs from a recently published study (10).

80 Our panel consisted of 8 mAbs: EM-2E01, 1000-1D05, 1000-3B04, 1000-3B06, 1000-3C05, 294-

81 16-009-A-1C02, 294-16-009-A-1D05 and 300-16-005-G-2A04. We also included a negative IgG

82 control antibody, KL-1C12, which targets the Ebola virus glycoprotein (34). Each mAb's

83 neuraminidase inhibition activity (NAI), measured using an enzyme-linked lectin assay (ELLA),

84 and neutralization activity, measured through a plaque reduction assay (PRNA), was first

85 determined against the wild type A/Netherlands/602/2009 H1N1 strain. All mAbs, aside from

86 1000-3C05 and 294-16-009-A-1D05, had NAI activity (**Table 1**). The mAb 300-16-005-G-2A04 did

87 not have neutralization activity, and mAbs 1000-3C05, 294-16-009-A-1C02, 294-16-009-A-1D05

88 had low neutralization activity (**Table 1**).

89 Escape mutant viruses (EMVs) were produced by passaging the wild type H1N1 virus with each

90 antibody in Madin Darby Kidney cells (MDCKs). We began with a multiplicity of infection (MOI)

91 of 0.01 and 0.25 times the 50% inhibitory concentration (IC_{50}) of each mAb. EMVs were

92 detected after 4-10 passages ($2 \times IC_{50}$ to $128 \times IC_{50}$) (**Table 2**). MAbs EM-2E01, 1000-3B04, 1000-

93 3C05, 294-16-009-A-1C02 and 300-16-005-G-2A04 generated 7 distinct EMVs. The NA

94 mutations identified were N88D (1000-3C05), N270D (1000-3B04), Q313K/R (294-16-009-A-

95 1C02), S364N (EM-2E01), S364N/N369T (EM-2E01) and R430Q (300-16-005-G-2A04) (**Table 2**).

96 Additionally, the irrelevant IgG control virus contained an NA mutation at D454G. We were

97 unable to generate viruses that escaped the mAbs 1000-1D05, 1000-3B06 and 294-16-009-A-

98 1D05 after 10 passages. The detected mutations are distributed in different regions of the NA
99 protein (**Figure 1**). S364N, N369T and R430Q are located on the top of the tetramer (**Figure 1A**).
100 N270D and Q313K/R are located on the side of the tetramer (**Figure 1B-C**). N88D is located on
101 the bottom of the tetramer, near the head/stalk interface (**Figure 1C**) and R430Q is the closest
102 to the NA enzymatic site. Mutations at N270 and N369 have also been identified using human
103 mAbs in other studies (10, 31). The mutations N88D, Q313K/R, S364N and R430Q have not
104 been previously identified using human mAbs. Each EMV and the irrelevant IgG control virus
105 shared several HA mutations and also contained mutations in other genomic segments (**Tables**
106 **2**).

107

108 **Escape mutant viruses are resistant to binding, NAI and neutralization activity of mAbs**

109 We next used the mAbs to evaluate the impact of each NA mutation on antibody binding, NAI
110 and neutralization activity. Using immunofluorescence assays we identified that the N270D
111 mutation impacted most of the antibodies in our panel, including those that produced other
112 EMVs (**Figure 2A**). The N88D mutation only affected the binding of the mAb that caused the
113 mutation, 1000-3C05. Q313K impacted binding of the mAb that caused that mutation (294-16-
114 009-A-1C02) and mAb 296-16-009-1D05 while Q313R only impacted the binding of 294-16-009-
115 A-1C02. S364N and the double mutation S364N/N369T affected the binding of EM-2E01 and
116 1000-1D05 (**Figure 2A**).

117 To determine changes in NAI activity, we performed ELLAs with each EMV in the presence of
118 each mAb. While 1000-3C05 has no NAI activity, we still assessed if the mutation it caused,
119 N88D, impacted any other antibodies in the panel. We found that it caused no significant

120 changes in the NAI activity of any of the mAbs tested (**Figure 2B**). We found that the N270D
121 mutation increased the NAI IC₅₀ values of the same mAbs that lost binding to the EMV,
122 including complete escape from 1000-3B04 and 294-16-009-A-1C02, along with resistance to
123 1000-3B06 (42-fold increase in NAI IC₅₀) and 300-16-005-G-2A04 (30-fold change in NAI IC₅₀)
124 (**Figure 2B, Table 3**). The Q313K mutation impacted the NAI activity of 1000-1D05 (13-fold
125 increase in NAI IC₅₀) and caused complete escape from 294-16-009-A-1C02. Q313R had less of
126 an impact on mAb NAI activity and caused complete escape from 294-16-009-A-1C02 without
127 causing resistance to other mAbs. S364N and the double S364N/N369T mutant led to complete
128 escape from EM-2E01. The mutation R430Q did not have a strong impact on any mAb NAI
129 activity (**Figure 2B**). We also identified a natural isolate, A/New York/PV01575/2018, which
130 contained mutations at residues identified in EMVs (N270K and N369K). This virus completely
131 escaped EM-2E01, 1000-3B04, 1000-3B06 and 300-16-005-G-2A04 (**Figure 2B**). No EMVs
132 showed increased resistance to the neuraminidase inhibitor oseltamivir (**Figure 2B, Table 3**).

133 We observed a more significant impact on mAb neutralization compared to NAI activity. This
134 may be caused by the mechanism of neutralization, which relies on strong NAI activity to
135 prevent virus spread and plaque formation. So, moderate changes in NAI activity would still
136 allow for the formation of plaques, increasing neutralizing IC₅₀ values. The N88D EMV
137 completely escaped mAbs 1000-3C05 and 300-16-005-G-2A04 (**Figure 2C, Table 4**). The N270D
138 EMV had complete escape from all mAbs in the panel aside from EM-2E01 (**Figure 2C, Table 4**).

139 Q313K led to escape from 1000-1D05, 1000-3B06, 1000-3C05, 294-16-009-A-1C02 and 300-16-
140 005-G-2A04. However, Q313R led to escape from 1000-1D05, 1000-3C05, 294-16-009-A-1C02
141 and 300-16-005-G-2A04 but did not impact the neutralization activity of 1000-3B06. S364N and

142 S364N/N369T EMVs completely escaped EM-2E01, 1000-1D05, 1000-3C05, 294-16-009-A-1C02
143 and 300-16-005-G-2A04 (**Figure 2C, Table 4**). A/New York/PV01575/2018 escaped all mAbs in
144 the panel aside from 294-16-009-A-1C02. We found that the R430Q “EMV” did not have
145 resistance to any mAbs in the panel, preventing us from classifying it as a true escape mutant
146 virus. Therefore, we do not think that R430Q is a critical residue for mAb escape, despite being
147 tolerated in the NA. Importantly, the irrelevant IgG control virus had similar NAI and
148 neutralization IC₅₀ values compared to wild type virus, indicating that the mutation D454G does
149 not directly impact mAb activity.

150

151 **Escape mutant viruses retain fitness *in vitro* and *in vivo***

152 Evaluating the fitness of each EMV is important to determine if natural isolates that acquire
153 these mutations will have a probability of showing increased or decreased fitness. We assessed
154 growth kinetics in two cell lines, MDCKs and A549 cells (derived from human lung epithelial
155 cells). In MDCK cells, EMVs aside from N270D had increased titers compared to the irrelevant
156 IgG control virus, with peak titers being 10-fold higher at 48 hours post infection (**Figure 3A**).
157 This pattern was similar in A549 cells, with N270D and R430Q EMVs replicating similarly to the
158 irrelevant IgG control viruses (**Figure 3C**). We also calculated the area under the curve (AUC) for
159 all EMVs. Using AUC values, we were able to determine that the N88D, Q313K, Q313R, S364N
160 and S364N/N369T EMVs had significantly higher growth kinetics in MDCK cells (**Figure 3B**). The
161 AUC calculations in A549 cells indicated that the N88D, Q313K, Q313R and S364N/N369T EMVs
162 also had significantly better growth kinetics in A549 cells (**Figure 3D**).

163 Additionally, we determined the mouse 50% lethal dose (mLD₅₀) of each EMV to assess fitness
164 changes *in vivo*. The irrelevant IgG control virus had a similar mLD₅₀ to the wild type virus, 7 and
165 1 plaque forming units (pfu), respectively (**Table 5**). This indicates that the irrelevant IgG control
166 virus G454D mutation is not influencing fitness *in vivo*. Since both Q313R EMV and S364N EMV
167 had similar changes in binding, NAI and neutralization activity to Q313K and S364N/N369T
168 EMVs, only one was chosen for mLD₅₀ experiments. A majority of EMVs had similar mLD₅₀
169 values as the irrelevant IgG control virus including the N88D, N270D, Q313K and S364N/N369T
170 EMVs (**Table 5**). The R430Q EMV had a moderate (45-fold) increase in mLD₅₀ (**Table 5**).
171 However, we also noted that this EMV contained a unique HA mutation, K226M, while the
172 other EMVs shared 3-4 HA mutations with the irrelevant IgG control virus. This data suggests
173 that mutations in the NA have less of an impact on viral fitness when compared to mutations in
174 the HA stalk(35). Overall, it appears that mutations that have impacts on binding, NAI and
175 neutralization activities may lead to increases of *in vitro* fitness however they do not
176 significantly change fitness of the virus *in vivo* in the mouse model.

177

178 **Discussion**

179 Our study has identified novel epitopes on the N1 targeted by human mAbs. Only 2 of the
180 escape mutations detailed here have been previously reported, N270 and N369, indicating that
181 these 2 residues are frequently targeted epitopes of human mAbs (10, 28, 31). Interestingly, a
182 majority of 2017-2018 isolates contained N270K and N369K mutations, which further
183 emphasizes their importance for mAb binding and NAI activity. The remaining mutations, N88D,
184 Q313K/R, S364N and R430Q, are part of newly identified mAb epitopes.

185 The mutation N88D, a critical residue for 1000-3C05, is located very close to the NA head-stalk
186 interface. MAb 1000-3C05 does not exhibit NAi activity and is poorly neutralizing, however,
187 previous reports have noted that it is protective *in vivo*, cross-reactive with several human N1s
188 (pre- and post-pandemic) and can utilize Fc-effector functions (10, 32). N88 is most likely not a
189 direct target of 1000-3C05 based on its location on the NA and may induce an allosteric change
190 to ablate mAb binding instead.

191 Mutations at Q313 were necessary for the evasion of 296-16-009-A-1C02 during escape
192 mutagenesis. Once the EMV was identified, we noted that this residue was also important for
193 another mAb in our panel, namely 1000-1D05. This residue is located on the side of the NA,
194 outside of any previously defined antigenic regions. We noticed that the Q313K mutation had a
195 slightly stronger effect on mAb escape compared to Q313R. This may be best explained by
196 amino acid biochemistry. The mutation from glutamine to asparagine does not change side
197 chain acidity/basicity however, lysine is a change from a neutral to a basic side chain.

198 We identified two separate EMVs containing the mutation S364N. When comparing escape
199 phenotypes, the S364N and S364N/N369T EMVs completely escaped the mAb EM-2E01,
200 became resistant to neutralization of 1000-1D05 and remained sensitive to the remaining mAbs
201 in the panel. These data suggest that S364N is sufficient for escape from EM-2E01 and that
202 N369T is not critical to mAb escape. Furthermore, the S364N mutation alone is responsible for
203 the introduction of an N-linked glycosylation, which is likely responsible for blocking mAb
204 activity. This is interesting because many recent isolates contain mutations at N369, like the
205 A/New York/PV01575/2018 isolate used in this study, but S364 is highly conserved.

206 The mutation G454D was identified in the irrelevant IgG control virus. However, this virus
207 behaved very similarly to wild type, indicating that this mutation does not significantly impact
208 viral fitness. To truly understand how these mutations impact NA antigenicity, it would be
209 important for future studies to test how human sera inhibit the neuraminidase activity of our
210 EMVs.

211 When combined with previous reports, we can conclude that human antibodies are targeting
212 more than just the enzymatic site (10, 31-33). **Figure 1** illustrates where the EMV mutations,
213 along with others discussed here, are located on the NA. Aside from overlaps at 248, 249, 270,
214 273, 309, 369, 451 and 456, the epitopes for murine mAbs are unique compared to what has
215 been observed for human mAbs. This highlights why it is important to evaluate antigenic sites
216 using human monoclonal antibodies to increase understanding of how the N1 is being targeted
217 by our immune responses.

218

219 **Methods**

220 *Cells, virus and antibodies*

221 MDCK cells (ATCC #CCL-34) and A549 cells (ATCC #CCL-185) were obtained from American Type
222 Culture Collection (ATCC) and propagated using cDMEM (1x Dulbecco's Modified Eagle Medium
223 [Gibco], 10% heat inactivated fetal bovine serum [Sigma-Aldrich], 1U/mL penicillin- 1µg/mL
224 streptomycin solution [Gibco] and 10mM 4-(2-hydroxyethyl)-1-piperazineethanesulfonic acid
225 [HEPES, Gibco]).

226 A/Netherlands/602/2009 (pdmH1N1) was grown in our laboratory by injection of 10-day old
227 specific pathogen free (SPF) embryonated chicken eggs (Charles River Laboratories) at 37°C for

228 2 days. All mAbs were identified and isolated previously and provided by Dr. Patrick Wilson
229 (University of Chicago) (10). They were expressed in our lab using the Expi293 transfection kit
230 according to the manufacturer's instructions (ThermoFisher). MAbs were purified through
231 gravity flow with protein G sepharose packed columns and concentrated as described
232 previously (36).

233 *Escape mutant generation*

234 Escape mutant viruses were generated using the H1N1 virus A/Netherlands/602/2009 as
235 maternal strain. MDCK cells (ATCC CCL-34) were plated at 6×10^5 cells/mL in a 12-well, sterile cell
236 culture plate and incubated overnight at 37°C with 5% CO₂. The following day, virus was diluted
237 to an MOI of 0.01 (1×10^3 pfu) in 1x minimal essential medium (1xMEM; 10% 10xMEM [Gibco],
238 2mM L- glutamine [Gibco], 0.1% sodium bicarbonate [Gibco], 10 mM HEPES, 1U/mL penicillin-
239 1µg/mL streptomycin solution, and 0.2% bovine serum albumin) supplemented with 1µg/mL
240 tolylsulfonyl phenylalanyl chloromethyl ketone (TPCK)-treated trypsin. Antibodies were then
241 added to the virus at a concentration that was 0.25 times the NAI IC₅₀. The virus and antibody
242 mixture was incubated for 1 hour at room temperature, shaking. MDCK cells were washed with
243 1x phosphate buffered saline (1xPBS, Gibco) and then the mixture was added to the cells. They
244 were then incubated at 37°C with 5% CO₂ for 2 days. Supernatant was collected stored at -80°C
245 until further use. For subsequent passages, MDCK cells were plated as described above and
246 infected with a 1:10 dilution of the previous passage in 1xMEM with TPCK-treated trypsin
247 (1µg/mL) and incubated for 40 minutes at 37°C with 5% CO₂. In the meantime, mAb was diluted
248 in 1xMEM with TPCK-treated trypsin to a concentration that was doubled from the previous
249 passage (0.25x, 0.5x, 1x and so on). After 40 minutes, diluted mAb was added to the virus

250 infected cells and left for 2 days at 37°C with 5% CO₂. Cell culture supernatant was screened for
251 escape mutant viruses through plaque assays with 128xI_{C50} of mAb present in the agarose
252 overlay. Individual plaques were chosen and propagated in SPF eggs for 2 days at 37°C as
253 described above.

254 *RNA isolation and deep sequencing*

255 RNA was isolated from egg allantoic fluid using the E.Z.N.A viral RNA extraction kit (Omega Bio-
256 Tek) according to the manufacturer's instructions and then underwent next generation
257 sequencing. Sequences were assembled using a pipeline designed at the Icahn School of
258 Medicine at Mount Sinai as described previously (37). To identify point mutations, full length
259 coding sequences were compared to the sequenced wild type A/Netherlands/602/2009 used
260 for escape mutagenesis.

261 *Plaque assay*

262 Plaque assays were performed using a standard protocol. MDCK cells were seeded 24 hours
263 prior at 8x10⁵ cells/mL. Next, virus samples were serially diluted in 1xMEM from 10⁻¹ to 10⁻⁶.
264 MDCK cells were washed with 1xPBS and then infected with 200µL of each virus dilution. Virus
265 was incubated for 40 minutes at 37°C with 5% CO₂, rocking every 10 minutes. Afterwards, virus
266 was aspirated and immediately replaced with 1mL of an agarose overlay containing 2xMEM,
267 0.1% (diethylaminoethyl)-dextran (DEAE), 1µg/mL TPCK-treated trypsin, and 0.64% Oxoid
268 agarose. Plates were incubated for 2 days at 37°C with 5% CO₂. Cells were then fixed using a
269 3.7% solution of paraformaldehyde (PFA) and incubated at 4°C overnight. To plaque
270 visualization, the overlay was removed and cells were stained with a solution containing 20%
271 methanol and 0.5% crystal violet.

272 *Immunofluorescence*

273 MDCK cells were plated at 3×10^5 cells/mL in a sterile, 96-well plate and incubated overnight at
274 37°C with 5% CO_2 . The following day, cells were checked for >99% confluency and washed with
275 1xPBS. Virus was diluted to an MOI of 5 in 1xMEM and added to each well (100 μL /well). Plates
276 were incubated overnight at 37°C with 5% CO_2 . The following day, cells were fixed using 200 μL
277 of 3.7% PFA and incubated overnight at 4°C . Next, the PFA was removed and cells were blocked
278 with 1xPBS containing 3% nonfat milk (American Bio) for 1 hour at room temperature. The
279 blocking solution was then removed and replaced 1% nonfat milk. Primary mAbs were diluted
280 to 300 μg in 1xPBS and added to the 1% milk at a 1:10 dilution, for a final concentration of 30 μg
281 per well. Primary antibodies were incubated for 1 hour at room temperature, shaking. Plates
282 were then washed 3 times with 1xPBS. Secondary antibody AlexaFluor™ 488 goat anti-human
283 IgG (H+L) (Invitrogen) was diluted to 1:500 in 1% milk, added and incubated for 1 hour at room
284 temperature, in the dark and shaking. The plates were then washed 3 times with 1xPBS. To
285 prevent cells from drying out, 50 μL of 1xPBS was added to each well. Plates were visualized
286 using the CELIGO S adherent cell cytometer (Nexcelom Bioscience) with the 2-channel Target
287 1+2 (merge) setting. Exposure time, gain and focus (set using image-based auto focus with the
288 488nm signal as the target) were automatically determined by the machine. Fluorescence was
289 calculated using the default analysis settings and percent fluorescence was determined based on
290 wild type signal. We performed 2 independent assays, however only representative images
291 from one assay are shown here.

292 *Enzyme-linked lectin assay (ELLA)*

293 We performed enzyme-linked lectin assays with each EMV and wild type virus to determine NA
294 activity. Flat bottom Immulon 4HBX microtiter plates (Thermo Scientific) were coated with
295 25µg/mL of fetuin (Sigma) diluted in 1xPBS, at 100µL per well, and incubated overnight at 4°C.
296 The next day, viruses were serially diluted (3-fold) in sample diluent buffer (1xPBS with 0.5mM
297 MgCl₂, 0.9mM CaCl₂, 1% BSA and 0.5% Tween 20) in a sterile 96-well plate. Once diluted, an
298 additional 1:1 ratio of sample diluent was added to the plate. This was incubated for 1 hour at
299 room temperature, shaking. After 1 hour, the fetuin coated plates were washed 3 times with
300 PBS containing 0.1% Tween 20 (PBS-T) using the AquaMax 3000 automated plate washer.
301 Diluted virus was immediately added to the plates and then incubated at 37°C, with 5% CO₂ for
302 18 hours (overnight). The following day, plates were washed 6 times with PBS-T. Peanut
303 agglutinin (PNA, Sigma) was diluted to 5µg/mL in conjugate diluent buffer (1xPBS with 0.5mM
304 MgCl₂, 0.9mM CaCl₂ and 1% BSA) and added to the washed plates. This was incubated for 2
305 hours in the dark at room temperature. The PNA was then removed and plates were washed 3
306 times with PBS-T. SigmaFast *o*-phenylenediamine dihydrochloride (OPD, Sigma) was diluted in
307 water. OPD was added at 100µL per well and incubated for 3 minutes at room temperature.
308 The reaction was stopped by adding 50µL of 3M hydrochloric acid and then absorbance (at
309 490nm) was immediately determined using Synergy H1 hybrid multimode microplate reader
310 (BioTek). PRISM 7.0 was used to determine the effective concentration of each virus that would
311 yield detectable NA activity. Each ELLA was done in triplicate.

312 *Neuraminidase inhibition assay (NAI assay)*

313 To determine NAI activity of each mAb, flat-bottom Immulon 4HBX microtiter plates (Thermo
314 Scientific) were coated with 25µg/mL fetuin (Sigma) diluted in 1xPBS and incubated overnight at

315 4°C. The following day, antibodies were diluted in sample diluent buffer to 120µg/mL and then
316 serially diluted 1:3 in a sterile 96-well plate. Virus was diluted to 2 times the effective
317 concentration determined in an ELLA and added to mAbs at a 1:1 ratio. This was incubated for 1
318 hour at room temperature, shaking. The fetuin coated plates were washed 3 times in PBS-T as
319 described above. Virus-mAb dilutions were transferred to the fetuin coated plates and
320 incubated at 37°C, with 5% CO₂, for 18 hours (overnight). The following day, we followed the
321 ELLA procedure described above. The 50% inhibitory concentration (IC₅₀) was determined using
322 PRISM 7.0. Each NAI assay was performed in duplicate. Significance between IC₅₀ values for
323 each EMV and the irrelevant IgG control virus were calculated using a 2-way ANOVA.

324 *Plaque reduction assay (PRNA)*

325 MDCK cells were plated at 8x10⁵ cells/mL in 12-well plates. The following day, mAbs were
326 diluted to 100µg/mL in 300µL 1xMEM and serially diluted 1:5 in 1xMEM to a final concentration
327 of 0.032µg/mL. Each virus was then diluted in 1xMEM to 1x10³ pfu and 50µL was added to each
328 antibody dilution. This virus-mAb mixture was incubated for 1 hour at room temperature,
329 shaking. Afterwards, MDCK cells were washed with 1xPBS and then immediately infected with
330 200µL per well of the virus-mAb mixture. The plates were incubated for 40 minutes at 37°C,
331 with 5% CO₂, rocking every 10 minutes. In the meantime, the overlay was prepared. Antibodies
332 were diluted to 100µg/mL in 625µL of 2xMEM and then serially diluted as described above. TA
333 solution containing 1xDEAE and 1µg/mL of TPCK-treated trypsin in sterile water for injection
334 (Gibco) was added at 180µL to each antibody dilution. When the infection finished, 360µL of 2%
335 Oxoid agarose was added the overlay mixture, in small batches to prevent solidification before
336 being transferred to cells. The inoculum was removed and immediately replaced with the

337 overlay so that the mAb dilution in the overlay was the same as the concentration in the
338 inoculum. The plates were then incubated at 37°C, with 5% CO₂, for 2 days. Cells were fixed and
339 stained as described above. Each PRNA was done in duplicate. Significance between
340 neutralizing IC₅₀ values for each EMV and the irrelevant IgG control virus were calculated using
341 a 2-way ANOVA.

342 *Growth kinetics*

343 MDCK cells were seeded at 8x10⁵ cells/mL in sterile, 24-well plates and incubated overnight at
344 37°C with 5% CO₂. The following day, virus was diluted to an MOI of 0.01 (5x10³ pfu) in 1xMEM
345 supplemented with 0.2µg/mL of TPCK-treated trypsin. Cells were washed with 1xPBS and then
346 immediately infected. A portion of the inoculum was reserved as the T0 control. The plates
347 were incubated for 72 hours and an aliquot was collected every 12 hours, for 72 hours total.
348 Virus titers were determined using plaque assays. Each growth curve was performed in
349 biological duplicates. AUC values were calculated using PRISM 7.0. Significance was determined
350 using a one-way ANOVA with the default PRISM settings.

351 *Mouse lethal dose (mLD₅₀)*

352 The mLD₅₀ for each EMV was determined using female BALB/c mice (at 6-8 weeks of age,
353 Jackson Laboratory) in accordance with protocols approved by the Institutional Animal Care and
354 Use Committee at the Icahn School of Medicine at Mount Sinai. Each virus was diluted from 10⁵
355 to 10¹ in 1xPBS and 3 mice per dilution were infected (50µL per mouse). Weight loss and
356 survival was monitored daily, for 14 days post infection. Mice that lost more than 25% of their
357 initial body weight were euthanized.

358

359 Acknowledgements

360 We thank the Mount Sinai Pathogen Surveillance Program for providing access to discard
361 nasopharyngeal swab specimen. This work was supported in part by the National Institute of
362 Allergy and Infectious Disease (NIAID) Centers of Excellence for Influenza Research and
363 Surveillance (CEIRS) contract (HHSN272201400008C and HHSN272201400005C).

364

365 Conflicts of Interest

366 The Icahn School of Medicine at Mount Sinai has filed patent applications regarding influenza
367 virus vaccines based on neuraminidase. FK is listed as coinventor.

368 References

- 369 1. Prevention CfDCa. 2020. Past Seasons Estimated Influenza Disease Burden.
370 <https://www.cdc.gov/flu/about/burden/past-seasons.html>. Accessed
- 371 2. Thompson WW, Weintraub E, Dhankhar P, Cheng PY, Brammer L, Meltzer MI, Bresee JS, Shay
372 DK. 2009. Estimates of US influenza-associated deaths made using four different methods.
373 *Influenza Other Respir Viruses* 3:37-49.
- 374 3. Shaw M, Palese P. 2013. Field's Virology, p 1151-1185. *In* Knipe DM HP (ed), 6 ed. Lippincott-
375 Raven, Philadelphia, PA.
- 376 4. Bouvier NM, Palese P. 2008. The biology of influenza viruses. *Vaccine* 26 Suppl 4:D49-53.
- 377 5. Nachbagauer R, Liu WC, Choi A, Wohlbold TJ, Atlas T, Rajendran M, Solórzano A, Berlanda-
378 Scorza F, García-Sastre A, Palese P, Albrecht RA, Krammer F. 2017. A universal influenza virus
379 vaccine candidate confers protection against pandemic H1N1 infection in preclinical ferret
380 studies. *NPJ Vaccines* 2:26.
- 381 6. McAuley JL, Gilbertson BP, Trifkovic S, Brown LE, McKimm-Breschkin JL. 2019. Influenza Virus
382 Neuraminidase Structure and Functions. *Front Microbiol* 10:39.
- 383 7. Air GM. 2012. Influenza neuraminidase. *Influenza and Other Respiratory Viruses* 6:245-256.
- 384 8. McMahon M, Kirkpatrick E, Stadlbauer D, Strohmeier S, Bouvier NM, Krammer F. 2019. Mucosal
385 Immunity against Neuraminidase Prevents Influenza B Virus Transmission in Guinea Pigs. *mBio*
386 10:e00560-19.
- 387 9. Grohskopf LA, Alyanak E, Broder KR, Walter EB, Fry AM, Jernigan DB. 2019. Prevention and
388 Control of Seasonal Influenza with Vaccines: Recommendations of the Advisory Committee on
389 Immunization Practices — United States, 2019–20 Influenza Season. *MMWR Recomm Rep* 68:1-
390 20.
- 391 10. Chen YQ, Wohlbold TJ, Zheng NY, Huang M, Huang Y, Neu KE, Lee J, Wan H, Rojas KT, Kirkpatrick
392 E, Henry C, Palm AE, Stamper CT, Lan LY, Topham DJ, Treanor J, Wrammert J, Ahmed R,

- 393 Eichelberger MC, Georgiou G, Krammer F, Wilson PC. 2018. Influenza Infection in Humans
394 Induces Broadly Cross-Reactive and Protective Neuraminidase-Reactive Antibodies. *Cell*
395 173:417-429.e10.
- 396 11. Wohlbold TJ, Nachbagauer R, Xu H, Tan GS, Hirsh A, Brokstad KA, Cox RJ, Palese P, Krammer F.
397 2015. Vaccination with Adjuvanted Recombinant Neuraminidase Induces Broad Heterologous,
398 but Not Heterosubtypic, Cross-Protection against Influenza Virus Infection in Mice. *mBio*
399 6:e02556-14.
- 400 12. Centers for Disease Control and Prevention NCflARDN. 2020. Past Seasons Vaccine
401 Effectiveness Estimates. <https://www.cdc.gov/flu/vaccines-work/past-seasons-estimates.html>.
402 Accessed
- 403 13. Office of the Associate Director for Communication DMB, Division of Public Affairs. October 14,
404 2016 2016. Seasonal Influenza Vaccine Effectiveness, 2005-2016. Accessed February 22.
- 405 14. Castilla J, Godoy P, Domínguez A, Martínez-Baz I, Astray J, Martín V, Delgado-Rodríguez M,
406 Baricot M, Soldevila N, Mayoral JM, Quintana JM, Galán JC, Castro A, González-Candelas F, Garín
407 O, Saez M, Tamames S, Pumarola T, Spain CCaCiIWG. 2013. Influenza vaccine effectiveness in
408 preventing outpatient, inpatient, and severe cases of laboratory-confirmed influenza. *Clin Infect*
409 *Dis* 57:167-75.
- 410 15. Puig-Barberà J, Arnedo-Pena A, Pardo-Serrano F, Tirado-Balaguer MD, Pérez-Vilar S, Silvestre-
411 Silvestre E, Calvo-Mas C, Safont-Adsua L, Ruiz-García M, Surveillance and Vaccine Evaluation
412 Group during the autumn 2009 H1N1 pandemic wave in Castellón Sa. 2010. Effectiveness of
413 seasonal 2008-2009, 2009-2010 and pandemic vaccines, to prevent influenza hospitalizations
414 during the autumn 2009 influenza pandemic wave in Castellón, Spain. A test-negative, hospital-
415 based, case-control study. *Vaccine* 28:7460-7.
- 416 16. Szilagyi PG, Fairbrother G, Griffin MR, Hornung RW, Donauer S, Morrow A, Altaye M, Zhu Y,
417 Ambrose S, Edwards KM, Poehling KA, Lofthus G, Holloway M, Finelli L, Iwane M, Staat MA,
418 Network NVS. 2008. Influenza vaccine effectiveness among children 6 to 59 months of age
419 during 2 influenza seasons: a case-cohort study. *Arch Pediatr Adolesc Med* 162:943-51.
- 420 17. Russell KL, Ryan MAK, Hawksworth A, Freed NE, Irvine M, Daum LT. 2005. Effectiveness of the
421 2003–2004 influenza vaccine among U.S. military basic trainees: a year of suboptimal match
422 between vaccine and circulating strain. 23:1981-1985.
- 423 18. Eichelberger MC, Morens DM, Taubenberger JK. 2018. Neuraminidase as an influenza vaccine
424 antigen: a low hanging fruit, ready for picking to improve vaccine effectiveness. 53:38-44.
- 425 19. Krammer F, Fouchier RAM, Eichelberger MC, Webby RJ, Shaw-Saliba K, Wan H, Wilson PC,
426 Compans RW, Skountzou I, Monto AS. 2018. NAction! How Can Neuraminidase-Based Immunity
427 Contribute to Better Influenza Virus Vaccines? *mBio* 9.
- 428 20. Krammer F, Li L, Wilson PC. 2019. Emerging from the Shadow of Hemagglutinin: Neuraminidase
429 Is an Important Target for Influenza Vaccination. 26:712-713.
- 430 21. Jagadesh A, Salam AAA, Mudgal PP, Arunkumar G. 2016. Influenza virus neuraminidase (NA): a
431 target for antivirals and vaccines. 161:2087-2094.
- 432 22. Gilchuk IM, Bangaru S, Gilchuk P, Irving RP, Kose N, Bombardi RG, Thornburg NJ, Creech CB,
433 Edwards KM, Li S, Turner HL, Yu W, Zhu X, Wilson IA, Ward AB, Crowe JE. 2019. Influenza H7N9
434 Virus Neuraminidase-Specific Human Monoclonal Antibodies Inhibit Viral Egress and Protect
435 from Lethal Influenza Infection in Mice. 26:715-728.e8.
- 436 23. Zhu X, Turner HL, Lang S, McBride R, Bangaru S, Gilchuk IM, Yu W, Paulson JC, Crowe JE, Ward
437 AB, Wilson IA. 2019. Structural Basis of Protection against H7N9 Influenza Virus by Human Anti-
438 N9 Neuraminidase Antibodies. 26:729-738.e4.
- 439 24. Maier HE, Nachbagauer R, Kuan G, Ng S, Lopez R, Sanchez N, Stadlbauer D, Gresh L, Schiller A,
440 Rajabathor A, Ojeda S, Guglia AF, Amanat F, Balmaseda A, Krammer F, Gordon A. 2019. Pre-

- 441 existing anti-neuraminidase antibodies are associated with shortened duration of influenza A
442 (H1N1)pdm virus shedding and illness in naturally infected adults. *Clin Infect Dis*.
- 443 25. Walz L, Kays SK, Zimmer G, von Messling V. 2018. Neuraminidase-Inhibiting Antibody Titers
444 Correlate with Protection from Heterologous Influenza Virus Strains of the Same Neuraminidase
445 Subtype. *J Virol* 92.
- 446 26. Memoli MJ, Shaw PA, Han A, Czajkowski L, Reed S, Athota R, Bristol T, Fargis S, Risos K, Powers
447 JH, Davey RT, Taubenberger JK. 2016. Evaluation of Antihemagglutinin and Antineuraminidase
448 Antibodies as Correlates of Protection in an Influenza A/H1N1 Virus Healthy Human Challenge
449 Model. *mBio* 7:e00417-16.
- 450 27. Wohlbold TJ, Chromikova V, Tan GS, Meade P, Amanat F, Comella P, Hirsh A, Krammer F. 2015.
451 Hemagglutinin Stalk- and Neuraminidase-Specific Monoclonal Antibodies Protect against Lethal
452 H10N8 Influenza Virus Infection in Mice. *J Virol* 90:851-61.
- 453 28. Wan H, Gao J, Xu K, Chen H, Couzens LK, Rivers KH, Easterbrook JD, Yang K, Zhong L, Rajabi M,
454 Ye J, Sultana I, Wan X-F, Liu X, Perez DR, Taubenberger JK, Eichelberger MC. 2013. Molecular
455 Basis for Broad Neuraminidase Immunity: Conserved Epitopes in Seasonal and Pandemic H1N1
456 as Well as H5N1 Influenza Viruses. *Journal of Virology* 87:9290.
- 457 29. Wan H, Yang H, Shore DA, Garten RJ, Couzens L, Gao J, Jiang L, Carney PJ, Villanueva J, Stevens J,
458 Eichelberger MC. 2015. Structural characterization of a protective epitope spanning
459 A(H1N1)pdm09 influenza virus neuraminidase monomers. *Nature communications* 6:6114-6114.
- 460 30. Jiang L, Fantoni G, Couzens L, Gao J, Plant E, Ye Z, Eichelberger MC, Wan H. 2015. Comparative
461 Efficacy of Monoclonal Antibodies That Bind to Different Epitopes of the 2009 Pandemic H1N1
462 Influenza Virus Neuraminidase. *Journal of virology* 90:117-128.
- 463 31. Gao J, Couzens L, Burke DF, Wan H, Wilson P, Memoli MJ, Xu X, Harvey R, Wrarmert J, Ahmed
464 R, Taubenberger JK, Smith DJ, Fouchier RAM, Eichelberger MC. 2019. Antigenic Drift of the
465 Influenza A(H1N1)pdm09 Virus Neuraminidase Results in Reduced Effectiveness of
466 A/California/7/2009 (H1N1pdm09)-Specific Antibodies. *mBio* 10.
- 467 32. Yasuhara A, Yamayoshi S, Kiso M, Sakai-Tagawa Y, Koga M, Adachi E, Kikuchi T, Wang IH, Yamada
468 S, Kawaoka Y. 2019. Antigenic drift originating from changes to the lateral surface of the
469 neuraminidase head of influenza A virus. *4:1024-1034*.
- 470 33. Stadlbauer D, Zhu X, McMahon M, Turner JS, Wohlbold TJ, Schmitz AJ, Strohmeier S, Yu W,
471 Nachbagauer R, Mudd PA, Wilson IA, Ellebedy AH, Krammer F. 2019. Broadly protective human
472 antibodies that target the active site of influenza virus neuraminidase. *Science* 366:499.
- 473 34. Duehr J, Wohlbold TJ, Oestereich L, Chromikova V, Amanat F, Rajendran M, Gomez-Medina S,
474 Mena I, tenOever BR, Garcia-Sastre A, Basler CF, Munoz-Fontela C, Krammer F. 2017. Novel
475 Cross-Reactive Monoclonal Antibodies against Ebolavirus Glycoproteins Show Protection in a
476 Murine Challenge Model. *J Virol* 91.
- 477 35. Kirkpatrick E, Carreno JM, McMahon M, Jiang K, van Bakel H, Wilson P, Krammer F. 2021.
478 Mutations in the HA stalk domain do not permit escape from a protective, stalk-based vaccine
479 induced immune response in the mouse model. *mBio* In press.
- 480 36. Tan GS, Krammer F, Eggink D, Kongchanagul A, Moran TM, Palese P. 2012. A Pan-H1 Anti-
481 Hemagglutinin Monoclonal Antibody with Potent Broad-Spectrum Efficacy In Vivo, p 6179-88, *J*
482 *Virol*, vol 86, 1752 N St., N.W., Washington, DC.
- 483 37. Mena I, Nelson MI, Quezada-Monroy F, Dutta J, Cortes-Fernández R, Lara-Puente JH, Castro-
484 Peralta F, Cunha LF, Trovão NS, Lozano-Dubernard B, Rambaut A, van Bakel H, García-Sastre A.
485 2016. Origins of the 2009 H1N1 influenza pandemic in swine in Mexico. *Elife* 5.
- 486 38. Li Q, Qi J, Zhang W, Vavricka CJ, Shi Y, Wei J, Feng E, Shen J, Chen J, Liu D, He J, Yan J, Liu H, Jiang
487 H, Teng M, Li X, Gao GF. 2010. The 2009 pandemic H1N1 neuraminidase N1 lacks the 150-cavity
488 in its active site. *17:1266-1268*.

489

490 **Tables**

491 **Table 1: NAI and neutralization activities of mAbs against wild type virus.** IC₅₀ values are
 492 shown in µg/mL. NA stands for not applicable.

mAb	NAI IC ₅₀	PRNA IC ₅₀
EM-2E01	0.02653	0.03427
1000-1D05	0.6385	2.663
1000-3B04	0.9519	3.659
1000-3B06	0.2702	0.1498
1000-3C05	>30	23.4
294-16-009-A-1C02	9.206	14.43
294-16-009-A-1D05	>30	35.52
300-16-005-G-2A04	0.0966	>100
1C12	NA	NA

493

494 **Table 2: Escape mutations identified in passaged viruses.** Specificity of each mAb was
 495 determined by referencing the previous publication characterizing these mAbs (10). Segments
 496 that are not listed did not contain any mutations. Numbering starts from the methionine of
 497 each protein. Mutations in bold are shared with the irrelevant IgG control virus.

EMV	mAb	Passages to Escape	NA Mutations	HA Mutations	PA Mutations	NP Mutations	M Mutations	NS1 Mutations
N88D	1000-3C05	8	N88D	R62K, D239G, R240Q	V100L	E372D	E204D	
N270D	1000-3B04	9	N270D	R62K, K136N, D239G, R240Q	V100L			
Q313K	294-16-009-A-1C02	4	Q313K	R62K, K136N, D239G, R240Q				
Q313R	294-16-009-A-1C02	4	Q313R	R62K, D239G, R240Q		S50N		
S364N	EM-2E01	6	S364N	R62K, D239G, R240Q	V100L			
S364N/N369T	EM-2E01	6	S364N/N369T	R62K,	V100L			

				D239G, R240Q				
R430Q	300-16-005- G-2A04	10	R430Q	K226M	V100L	S50N		
D454G	1C12	10	D454G	R62K, K163N, D239G, R240Q	V407I			G179R, I198L

498

499 **Table 3: NAI IC₅₀ values for mAbs against all EMVs.** IC₅₀ values are shown in µg/mL. 30 µg/mL

500 was the highest mAb concentration tested. Bolded values indicate significant differences in

501 IC₅₀s between the irrelevant IgG control virus and the EMV (*p<0.05).

EMV	EM- 2E01	1000- 1D05	1000- 3B04	1000- 3B06	294-16-009- A-1C02	300-16-005 - G-2A04	Oselta mivir
Irrelevant IgG Control Virus	0.012	0.076	0.543	0.154	5.652	0.059	0.083
N88D	0.018	0.078	0.696	0.226	12.030	0.067	0.051
N270D	0.014	0.503	>30*	11.250	>30*	2.968	0.088
Q313K	0.032	8.502	1.663	0.453	>30*	0.159	0.151
Q313R	0.015	0.113	0.774	0.190	>30*	0.066	0.070
S364N	>30*	0.898	1.017	0.320	11.770	0.125	1.249
S364N/N369T	>30*	1.605	2.039	0.291	8.053	0.129	2.622
R430Q	0.019	0.140	1.054	0.242	8.563	0.107	0.056
A/New York/PV01575/2018 N270K/N369K	>30*	0.040	>30*	>30*	19.790	>30*	0.064

502

503 **Table 4: Neutralization IC₅₀ values for mAbs against all EMVs.** Values were determined using

504 PRNAs. IC₅₀ values are shown in µg/mL. 100 µg/mL was the highest mAb concentrated tested.

505 Bolded values indicate significant differences in IC₅₀s between the irrelevant IgG control virus

506 and the EMV (*p<0.05).

EMV	EM- 2E01	1000- 1D05	1000- 3B04	1000- 3B06	1000- 3C05	294-16-009- A-1C02	294-16-009- A-1D05
Irrelevant IgG Control Virus	0.0300	0.341	0.8447	0.2041	14.98	5.592	22.34
N88D	0.0866	11.4	2.646	0.4076	100	25.56	100
N270D	0.0457	>100*	>100*	>100*	100	>100*	100
Q313K	0.2807	>100*	15.21	>100*	100	>100*	100

Q313R	0.1557	>100*	4.322	3.477	100	>100*	100
S364N	>100*	>100*	4.098	1.196	100	>100*	100
S364N/N369T	>100*	>100*	4.504	0.8054	100	>100*	100
R430Q	0.0320	0.0706 9	0.3104	0.1467	1.216	5.683	12.03
A/New York/PV01575/2018 N270K/N369K	>100*	>100*	>100*	>100*	100	24.4	100

507

508 **Table 5: EMVs have similar mLD₅₀ values as the irrelevant IgG control virus.** Values are listed
509 as pfu/mouse.

EMV	mLD ₅₀
A/Netherlands/602/2009	1
Irrelevant IgG Control Virus	7
N88D	6
N270D	18
Q313K	8
S364N/N369T	2
R430Q	316

510

511 Figure Legends

512 **Figure 1: Escape mutations mapped onto a three-dimensional structure of the NA.** The NA of
513 A/California/04/2009 (PDB ID 3NSS(38)) is depicted as a tetramer with 3 monomers colored in
514 light grey and one colored in darker grey. The darker grey subunit has residues identified by
515 previous publications and the NA active site (in white). Murine epitopes are illustrated in blue
516 (28), magenta (29) and yellow (30). Human epitopes are indicated in orange (10), purple (32),
517 green (31) and indigo (33). Mutations identified in the EMVs used for this study are highlighted
518 in red and identified using arrows. Views from the top **(A)**, side **(B)** and bottom **(C)** of the NA are
519 depicted.

520

521 **Figure 2: MAbs exhibit changes in binding, NAI and neutralizing activity towards EMVs. A)**

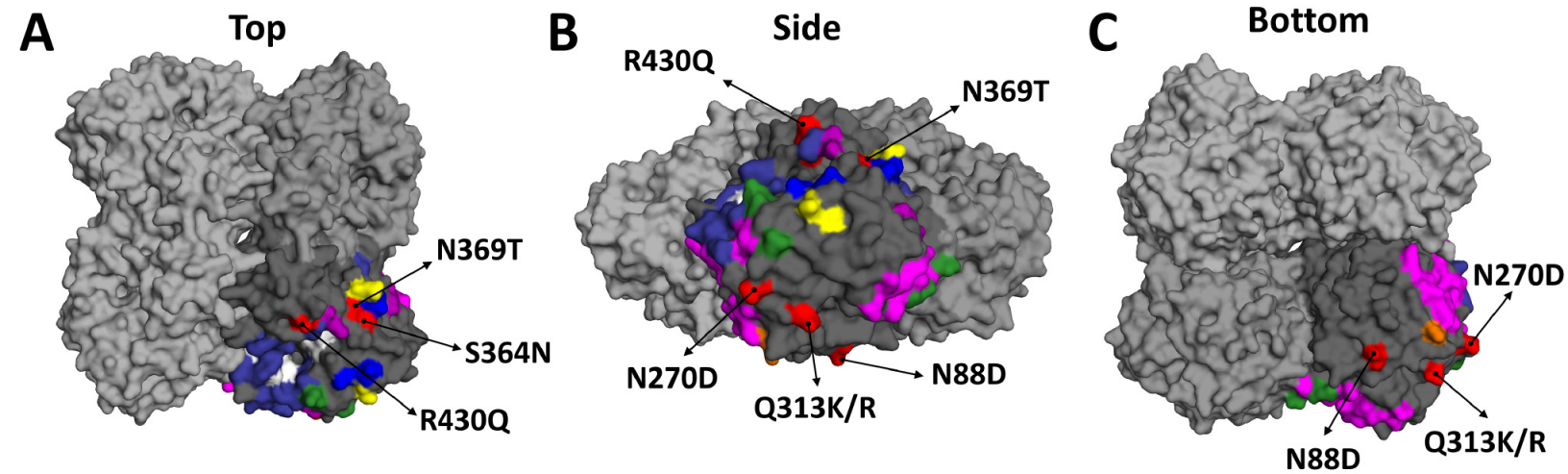
522 Immunofluorescence assay comparing binding of each mAb to wild type and EMVs. On the left
523 are representative images and the right shows a heat map of percent luminescence compared
524 to wild type. On the heat map, high binding is indicated by darker blue shading. Heat maps of
525 NAI **(A)** and neutralization IC₅₀s **(C)** of each mAb against wild type and EMVs. Each EMV is listed
526 on the X-axis while mAbs are listed on the Y-axis. Darker blue is a higher IC₅₀, which indicates
527 stronger escape phenotypes. Binding, NAI and neutralization assays were conducted in
528 duplicate.

529

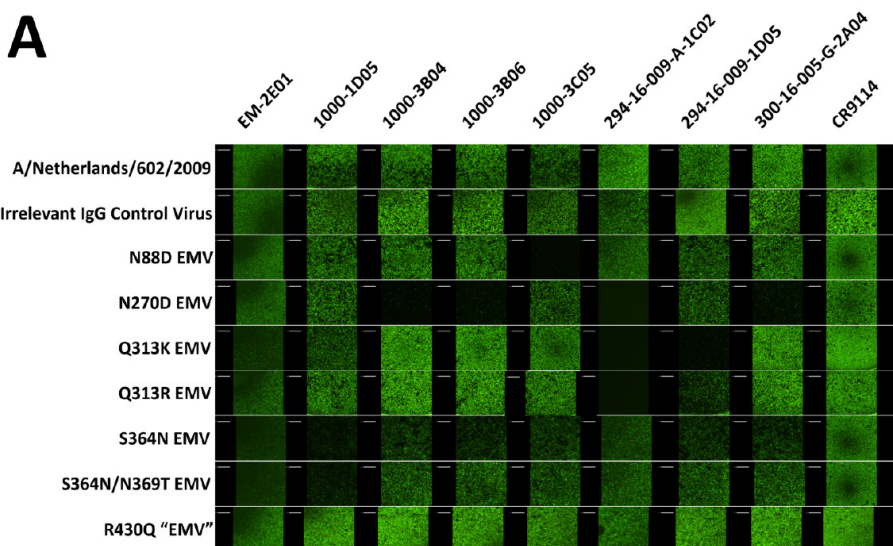
530 **Figure 3: EMVs have an increased growth phenotype *in vitro*.** EMVs' growth curves and their

531 corresponding AUC values are shown for MDCK **(A-B)** and A459 **(C-D)** cell lines. Samples were
532 collected every 12 hours. Time 0 is a measurement of starting inoculum titers. The significance
533 between AUC values for EMVs compared to the irrelevant IgG control virus are indicated on the
534 figure (**p<0.01, ***p<0.001 and ****p<0.0001). Figures show the mean with standard
535 deviations indicated by error bars, when applicable.

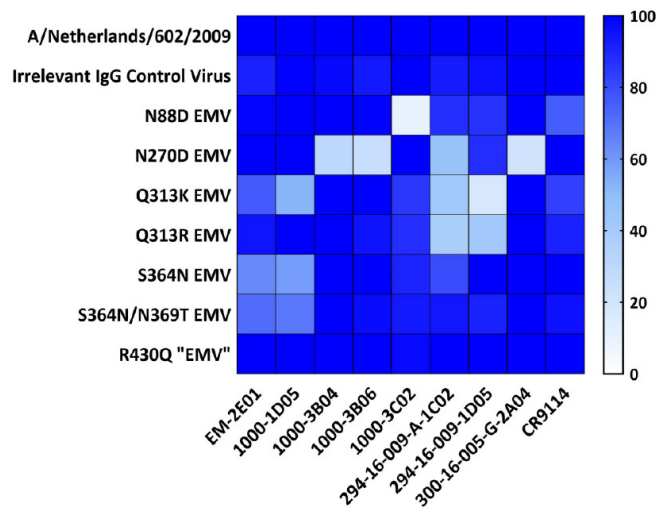
536



A

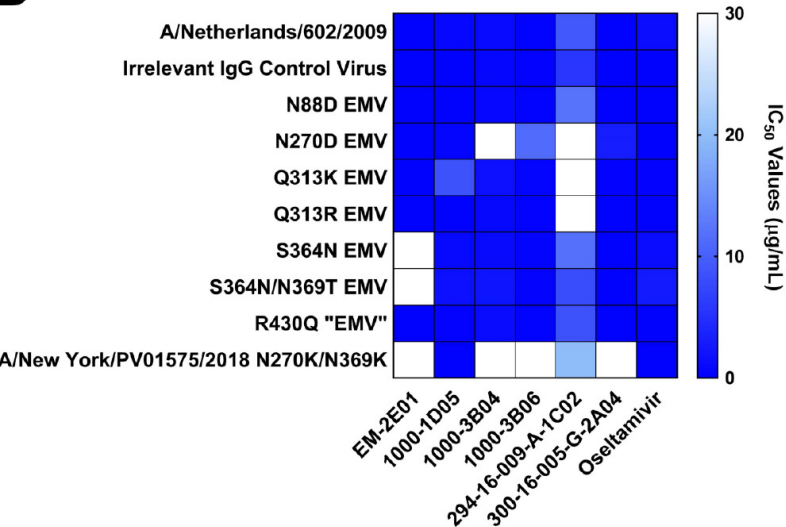


Percent Immunofluorescence



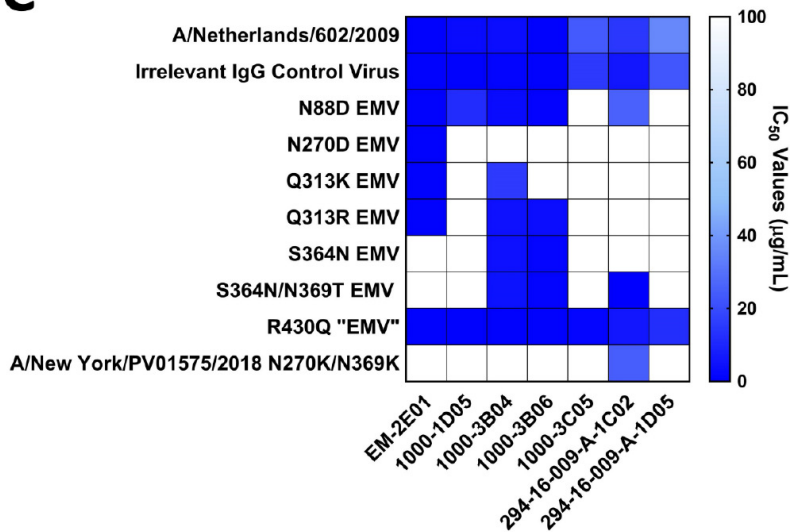
B

Neuraminidase Inhibition Activity

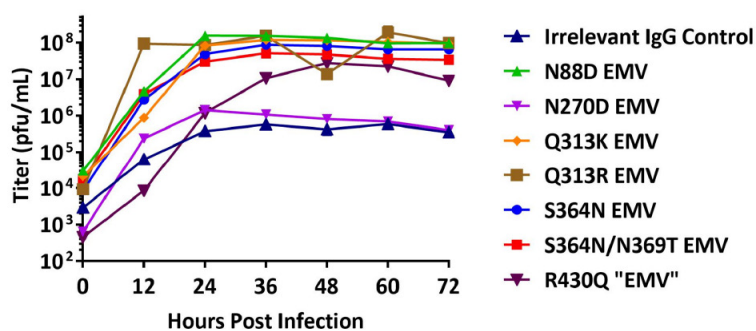


C

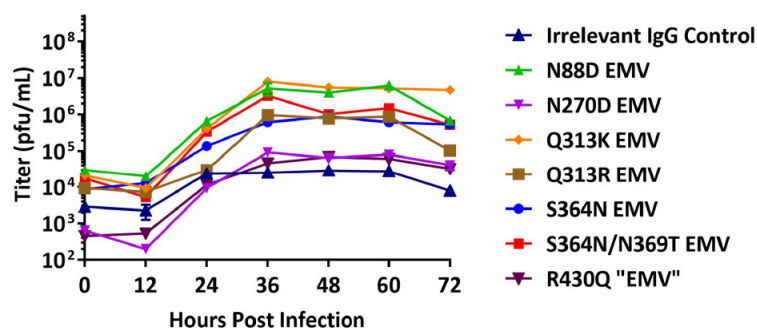
Neutralization Activity



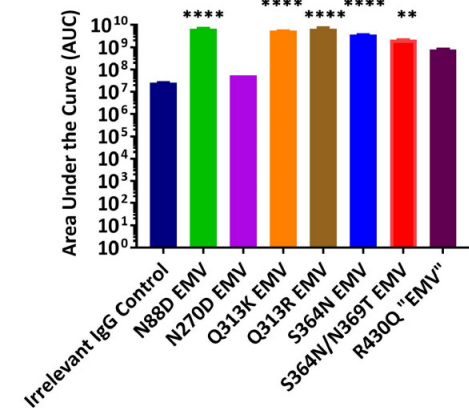
A MDCK Growth Kinetics



C A549 Growth Kinetics



B AUC in MDCK Cells



D AUC in A549 Cells

